

# Amorphous dysprosium carbonate: characterization, stability, and crystallization pathways

Beatriz Vallina · Juan Diego Rodriguez-Blanco ·  
Andrew P. Brown · Jesus A. Blanco ·  
Liane G. Benning

Received: 10 August 2012 / Accepted: 12 January 2013  
© Springer Science+Business Media Dordrecht 2013

**Abstract** The crystallization of amorphous dysprosium carbonate (ADC) has been studied in air (21–750 °C) and in solution (21–250 °C). This poorly ordered precursor,  $\text{Dy}_2(\text{CO}_3)_3 \cdot 4\text{H}_2\text{O}$ , was synthesized in solution at ambient temperature. Its properties and crystallization pathways were studied by powder X-ray diffraction, Fourier transform infrared spectroscopy, scanning and transmission electron microscopy, thermogravimetric analysis, and magnetic techniques. ADC consists of highly hydrated spherical nanoparticles of 10–20 nm diameter that are exceptionally stable under dry treatment at ambient and high temperatures (<550 °C). However, ADC transforms in solution to a variety of Dy-carbonates, depending on

the temperature and reaction times. The transformation sequence is (a) poorly crystalline metastable tengerite-type phase,  $\text{Dy}_2(\text{CO}_3)_3 \cdot 2-3\text{H}_2\text{O}$ ; and (b) the orthorhombic kozoite-type phase  $\text{DyCO}_3(\text{OH})$  at 165 °C after prolonged times (15 days) or faster (12 h) at 220 °C. Both the amorphous phase and the kozoite-type phase  $\text{DyCO}_3(\text{OH})$  are paramagnetic in the range of temperatures measured from 1.8 to 300 K.

**Keywords** Amorphous materials · Rare earths · Dysprosium · Carbonate · Crystallization

## Introduction

The crystallization of many simple ionic salts at ambient conditions usually follows complex reaction pathways, which are often initiated by the nucleation and growth of poorly ordered (often termed amorphous), metastable, and highly hydrated precursors. These amorphous precursors are thermodynamically unstable and often transform into crystalline, but metastable intermediate phases before finally crystallizing into the thermodynamically stable solid end-products (Meldrum and Cölfen 2008). Most of the research on such amorphous precursors has been focused on their compositional-dependent stabilities and on their formation and transformation conditions (i.e., amorphous calcium carbonates (Radha et al. 2010; Goodwin et al. 2010; Bolze et al. 2002; Rodriguez-Blanco et al. 2008) and amorphous calcium

**Electronic supplementary material** The online version of this article (doi:10.1007/s11051-013-1438-3) contains supplementary material, which is available to authorized users.

B. Vallina · J. D. Rodriguez-Blanco · L. G. Benning (✉)  
School of Earth and Environment, University of Leeds,  
Leeds LS2 9JT, UK  
e-mail: l.g.benning@leeds.ac.uk

B. Vallina  
e-mail: beatrizvallina@gmail.com

B. Vallina · J. A. Blanco  
Departamento de Física, Universidad de Oviedo, 33007  
Oviedo, Spain

A. P. Brown  
Institute for Materials Research, SPEME, Faculty of  
Engineering, University of Leeds, LS2 9JT, UK

phosphates (Zyman et al. 2010; Combes and Rey 2010). However, there are also salt systems where such amorphous precursors do either not crystallize even after very long time periods (Roncal-Herrero et al. 2009; Tobler et al. 2009) or where the formation of the thermodynamically stable end phase does not require an amorphous precursor as an initiators for the crystallization process (e.g., calcium sulfate, Van Driessche et al. 2012; La and Nd-phosphates, Roncal-Herrero et al. 2011). For example, amorphous silica when precipitated from solution (Tobler et al. 2009; Tobler and Benning 2011) is stable for extremely long times without crystallizing, while in the La and Nd-phosphate system (Roncal-Herrero et al. 2011) no amorphous precursor has so far been observed. However, in some salt systems, the formation of an amorphous precursor may at times be missed because the crystallization rates may be very rapid, as shown for the calcium carbonate systems (Bolze et al. 2002; Bots et al. 2012).

Interestingly, however, such amorphous precursor phases are important for various industrial applications as their composition and stability can be tailored for various uses (McHenry et al. 1999; Bauer et al. 2011). Among the more recent extremely high-interest amorphous phases are the rare-earth element (REE) phases, which have more and more uses in our daily lives (Bauer et al. 2011; Zhang et al. 2007) in a plethora of industrial applications (McHenry and Laughlin 2000), yet about which relatively little is known. This is surprising because although the stability of REE-bearing glassy alloys at high temperature (Buschow 1984) has been described, there is a gap in our knowledge about the formation of amorphous REE materials from solution at ambient temperature using a “green” approach. This is particularly important due to the role REE play in a wide variety of crucial electronic devices and clean energy emerging technologies in our society arising from the 4f electronic configuration of the REE ions (Xu et al. 2003; Kanamori 2006; Huang 2010).

Rare-earth elements are not abundant in the Earth crust and their supply for industrial needs is becoming constrained at the same time as the demand grows. This is a problem, which is raising several economic and politic concerns, specifically as more than 90 % of the global supply of REE comes from a single REE deposit in China (Bayan Obo deposit; Yang et al. 2011). This deposit contains a variety of ore minerals,

many of them are REE-bearing carbonates which are most often formed through magmatic or hydrothermal processes (Jones and Wall 1996). Owing to their economical importance, the understanding of the origin and distribution of such REE-bearing deposits has become a priority. However, the lack of basic data related to the identification and quantification of the processes and pathways that lead to the formation of REE-bearing minerals is hampering understanding.

Among all REEs, according to the US Department of Energy (Bauer et al. 2011), dysprosium (Dy) has been identified as the most critically needed rare-earth element. This deficit of Dy may affect clean energy technology development in the short (present—2015) and medium (2015–2025) term, followed by neodymium, terbium, europium, and yttrium. For example, between 2001 and 2011, the price of Dy has increased by  $\sim 5,000$  % in line with all other REE. Dysprosium’s prime clean energy use is as an additive to permanent magnets and superconducting compounds (Gasgnier 1991) for wind turbine generators and electric vehicle motors (Bauer et al. 2011). Dy is also used in specialized ceramics, high-intensity lighting devices, laser glassware, or luminescent materials in fluorescent lamps, etc. (Bünzli and Piguet 2005), yet little is known about how Dy phases form.

Although several REE carbonates have been synthesized and characterized in the last decade (Adachi et al. 2010; Song and Rongjun 2006; Refat 2004; Firsching and Mohammadzadei 1986; Leskelä and Niinistö 1986) in the case of Dy-bearing carbonates, the only reported crystal structures are for orthorhombic and hexagonal dysprosium carbonate hydroxides ( $\text{DyCO}_3(\text{OH})$ ; Tahara et al. 2007; Michiba et al. 2011; Kutlu and Meyer 1999; Doert et al. 1999) and dysprosium oxide carbonate ( $\text{Dy}_2\text{O}_2\text{CO}_3$ ; Kutlu and Meyer 1999). All were hydrothermally synthesized and characterized by X-ray diffraction, IR spectroscopy, thermogravimetric analyses, and magnetic measurements (Tahara et al. 2007; Salavati-Niasari et al. 2010; Christensen 1973; Caro et al. 1972; Charles 1965). However, the information about the pathways of their crystallization is scarce. So far, the characterization of these REE carbonates has only been carried out at a basic level because they are usually obtained as secondary products in the course of a synthesis of other more stable Dy compounds (e.g.,  $\text{Dy}_2\text{O}_3$ , Dy-bearing organics, etc.). Often the characterization of a product identified at a specific

time of reaction is done in isolation, i.e., the question of whether it is an end product, a precursor, or an intermediate phase has not been addressed. Currently, it is also not known if dysprosium carbonates (a) form via an amorphous precursor, (b) what is the stability, hydration, and properties of this potential amorphous precursor, and (c) what are the transformation pathways to crystalline Dy-bearing carbonates.

The characterization of these processes and a quantitative assessment of the crystallization pathways of Dy-bearing carbonates precipitated from solution, is not just a crucial missing link for their potential industrial applications (Yan et al. 2011), but such “green” low temperature aqueous solvent carbonate crystallization reactions can also contribute to the debate about the validity of the classical nucleation theory in the carbonate system overall (Meldrum and Sear 2008).

In this study, we have investigated the formation of Dy-carbonates from aqueous solution and characterized their stability and transformation pathways in air and in solution over a range of temperatures. Applying a variety of solid-state (X-ray diffraction and magnetic susceptibility), spectroscopic (FTIR), and microscopic (electron microscopy) techniques, we show that Dy-carbonate compounds form via the crystallization of an initial amorphous dysprosium carbonate (ADC) precursor. This precursor phase can remain stable when treated under dry conditions, but when aged in aqueous solution (depending on temperature and reaction conditions) its crystallization results in various intermediate metastable or stable dysprosium carbonate or dysprosium oxide phases.

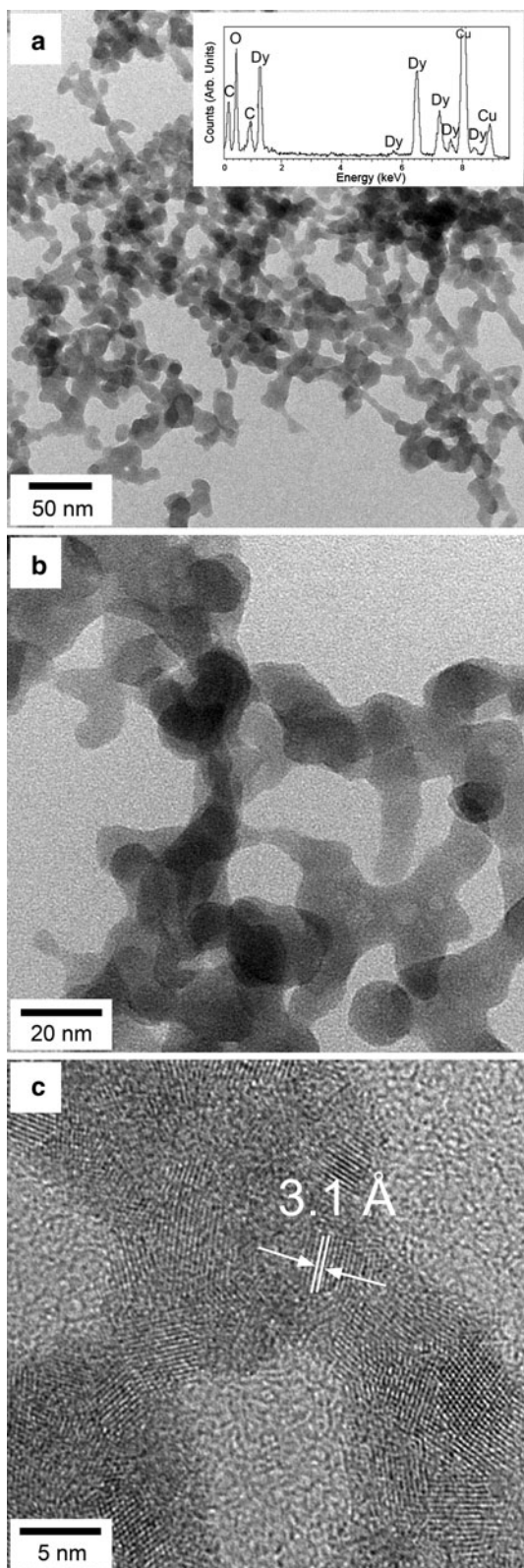
## Experimental

Dysprosium carbonates were synthesized by adding a 50 mM solution of  $\text{DyCl}_3 \cdot \text{H}_2\text{O}$  (Alfa Aesar, 99 % purity; pH = 4.98) to a 50 mM  $\text{Na}_2\text{CO}_3$  solution (Fisher Scientific, 99.9 % purity; pH = 11.20) at room temperature (21 °C) under constant and continuous stirring. Immediately after mixing, a white gel-like precipitate formed and the pH value rapidly dropped to 7.60 and stabilized (See Supplementary Information Fig. S1). Aliquots of this material were treated by three different approaches. One batch was reacted in air from 25 to 750 °C using thermodiffraction and an oven-chamber with heating occurring at a constant heating

rate of 1 °C/minute (hereafter termed: *dry-heated*). In addition, we dry heated aliquots at specific temperatures (220 and 300 °C) in an oven for 2 h to produce samples for diffraction and spectroscopic characterization of possible intermediate stages. The two other batches were aged in their native solution either at 21 °C for up to two months (*ambient*), or hydrothermally at 90, 165, or 220 °C for up to 15 days (*hydrothermal*). The hydrothermal treatments were carried out in Teflon-lined stainless steel (40 mL) vessels at saturated water vapor pressures.

The initial white gel, various intermediate products as well as the reaction products at the end of each treatment were if needed quenched to room temperature and vacuum filtered through 0.2- $\mu\text{m}$  polycarbonate membranes. The resulting solids were washed with water and isopropanol following the method described in Rodriguez-Blanco et al. (2008). All solid phases were characterized by powder X-ray diffraction (XRD), Fourier transform infrared spectroscopy (FTIR), and scanning electron microscopy (SEM). The dried white, gel-like material that formed immediately after solution mixing was also characterized by thermogravimetry, high-resolution microscopy, and X-ray thermodiffraction. Finally, owing to the well-known special magnetic properties of Dy-bearing compounds (Gasgnier 1991; Bünzli and Piguet 2005) the magnetic susceptibility of selected samples was also measured.

Conventional powder XRD patterns were collected using a Bruker D8 powder X-ray diffractometer ( $\text{CuK}\alpha_1$ ;  $2\theta$  range 10–75; 0.005°/step and 0.1 s/step), while powder X-ray thermodiffraction was carried out under atmospheric conditions using a Panalytical X'Pert Pro diffractometer equipped with an Anton Paar HTK 1200N High-Temperature Oven-Chamber ( $\text{CuK}\alpha_{1,2}$ ;  $2\theta$  range 20–50 at 0.01°/step and 0.16 s/step; constant heating rate of 1 °C/min from 25 to 750 °C). Crystallite sizes were estimated from the diffraction patterns using the Scherrer equation (Patterson 1939) with the assumption that the particles were stress-free and with pattern-matching refinement of the crystalline phases carried out by the Rietveld refinement software TOPAS (Coelho 2003). Furthermore, all crystallite sizes were calculated taking into account the X-ray pattern of a silicon standard ( $2\theta_{111} = 28.46^\circ$  and  $\text{FWHM} = 0.049^\circ$ ). FTIR spectra were recorded on an A2-Technology Microlab Portable mid-IR spectrometer with a Diamond internal reflection cell (DATR). The spectra were collected by



◀ **Fig. 1** **a, b** TEM images of the amorphous precursor phase. The *inset* shows EDX spectrum of the amorphous phase (the Cu background comes from the Cu support grid). Standard less quantification of this spectrum gives a Dy:O atomic ratio of 2:8. **c** TEM image of Dy<sub>2</sub>O<sub>3</sub> crystallized as a result of prolonged exposure to the electron beam of the TEM (see text)

adding 1024 scans in the 650–4,000 cm<sup>-1</sup> range at a resolution of 4 cm<sup>-1</sup>. The Thermo Nicolet OMNIC ESP 5.1 software package was used to manipulate the spectra, including baseline subtraction. Thermogravimetric analyses (TGA) were carried out using a Mettler TA 4000 instrument, while heating the samples from 25 to 1,000 °C at a rate of 10 °C/min in a nitrogen atmosphere. Images of the solids were acquired with a field emission gun scanning electron microscope (FEG-SEM, LEO 1530 Gemini, operated at 3 kV, and with an in-lens detector, equipped with an energy-dispersive X-ray (EDX) analysis system; Isis) and a FEG-transmission electron microscope (FEG-TEM; FEI CM200; operated at 197 kV and equipped with an Oxford Instruments energy-dispersive X-ray (EDX) analysis system (Isis) and a Gatan Imaging Filter (GIF-200)). Direct current (DC) magnetic susceptibility and magnetization as a function of field (H) were measured using a Quantum Design PPMS magnetometer. DC susceptibility was recorded under applied magnetic fields of 50 Oe and 1 kOe in the temperature range between 2 and 300 K, while magnetization as a function of field (H) was recorded in the -85 to 85 kOe range and from 2 to 300 K after cooling the sample in zero field.

## Results and discussion

### Amorphous dysprosium carbonate (ADC) and its dry crystallization

High-resolution TEM images of the air dried, white, gel-like phase that formed immediately upon mixing of the starting solutions revealed that it consisted of roughly spherical nanoparticles with diameters between 10 and 20 nm (Fig. 1a, b). The particles rapidly crystallized when exposed even for a few seconds to the electron beam of the TEM (Fig. 1c). However, dark field images recorded at a low electron fluence (to minimize the alteration), clearly showed that the particles were mostly amorphous and standardless quantification of EDX



spectra from the amorphous particles revealed a Dy:O atomic ratio of 2:8. Nevertheless, the presence of minor nanocrystallites (<a few nm) among the amorphous particles cannot be excluded. When the amorphous nanoparticles were crystallized under the beam, the resulting nanocrystals had lattice images with interplanar spacings of  $\sim 3.1$  Å. These correspond to the (222) *d*-spacing of crystalline Dy<sub>2</sub>O<sub>3</sub>. This ratio was also confirmed by quantification from EDX spectra after prolonged exposure of the amorphous precursor and its crystallization (Fig. 1c) which revealed that compared to the 2:8 Dy:O ratio in the amorphous starting material, the relative amount of O decreased in the crystalline product, reaching a  $\sim 2:3$  Dy:O ratio, as typical for Dy<sub>2</sub>O<sub>3</sub>.

Bulk powder X-ray diffraction of this initial amorphous material (Fig. 2 bottom pattern) showed three broad humps centered at  $\sim 20$ , 30, and 45°  $2\theta$  (marked with \*), consistent with the amorphous nature of the material identified by TEM. *Dry heating* this amorphous phase from 25 to 550 °C with simultaneous recording of thermodiffraction patterns, showed that it remained amorphous with no Bragg peaks forming across this temperature range (lower 3 patterns in Fig. 2). The only observed change was in a reduction in width and a minor increase in intensity of the 30° broad hump, compared to the room temperature pattern. This broad hump transforms about 550 °C to a crystalline Bragg peak identified

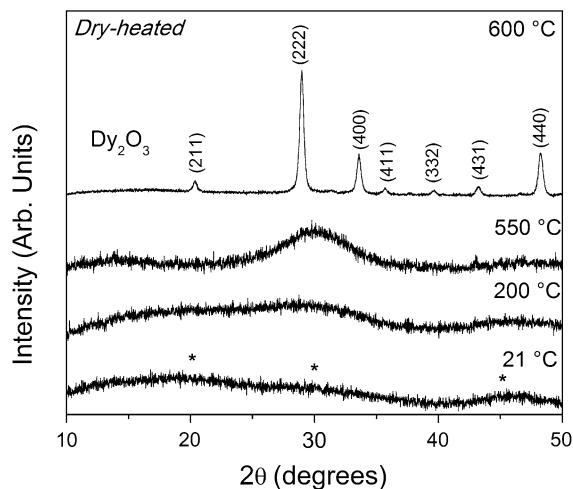


**Fig. 2** Selected powder X-ray diffraction patterns recorded from the solid precursor phase when *dry-heated* from 25 to 750 °C. The *asterisks* in the *bottom* pattern indicate the position of the humps in the amorphous precursor

as Dy<sub>2</sub>O<sub>3</sub> (Fig. 2, upper pattern), again confirming the TEM observations. Once initiated, the transformation from the amorphous starting material to Dy<sub>2</sub>O<sub>3</sub> in the dry state was complete within <50 °C (by  $\sim 600$  °C; Fig. 2, top pattern indexed to ICDD PDF 22-0612).

The true composition of the amorphous material was, however, only revealed through the analyses of the FTIR vibrations. The FTIR spectrum of the dry amorphous material (Fig. 3; bottom spectrum) was characterized by bands typical for carbonate and O–H vibrations, suggesting that the amorphous material was a highly hydrated amorphous dysprosium carbonate. This phase will for simplicity, hereafter be called ADC, in line with other amorphous carbonates in the literature (e.g., amorphous calcium carbonate (ACC); Radha et al. 2010; Rodriguez-Blanco et al. 2008; Brečević and Nielsen 1989). The most intense vibrations in our ADC, were located between  $\sim 1,500$  and  $700$  cm<sup>-1</sup> (marked with band numbers 2–8; detailed assignments see Supplementary Information Table S1) and most of these bands represent the main stretching vibrations of the carbonate ions (Farmer 1974). The other prominent feature in the ADC spectrum was the broad band between  $\sim 2,500$  and  $3,700$  cm<sup>-1</sup> (marked with band number 1). This broad band is typical for O–H stretching vibrations and corresponds to structural water (Farmer 1974). As shown above (Fig. 2) in the thermodiffraction data, the dry ADC powder remained stable below 550 °C.

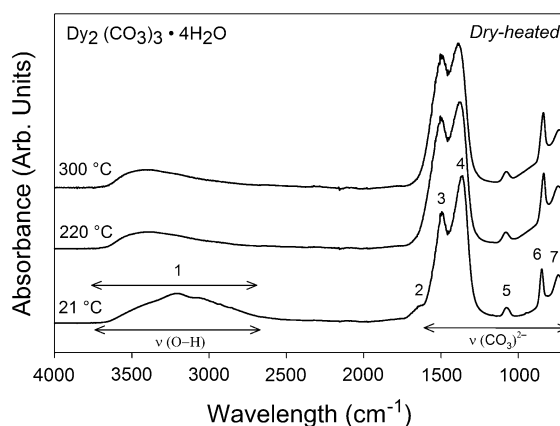


**Fig. 3** FTIR spectra of dried samples of Dy<sub>2</sub>(CO<sub>3</sub>)<sub>3</sub>·4H<sub>2</sub>O at 21 °C and after *dry-heated* treatment at 220–300 °C. The modes of vibrations are identical to those found for Dy<sub>2</sub>(CO<sub>3</sub>)<sub>3</sub>·4H<sub>2</sub>O (Fig. 3; table S1). Details of the band assignments are discussed in Table S1 and the text

We confirmed this stability by dry heating the ADC powder at 200 and 300 °C for 2 h and reanalyzing with FTIR. The resulting patterns (Fig. 3, upper two spectra) show that except for a minor decrease in intensity of the O–H stretching band no change in the vibrational spectra after heating was observed.

This combined datasets clearly suggest that under dry conditions, the precipitate that formed upon solution mixing is a strongly hydrated, ADC, that is extremely stable, and that does not crystallize upon dry heating <550 °C. Above this temperature, the ADC crystallized through a loss of water and carbonate ions directly to a dysprosium oxide. However, no other crystalline dysprosium carbonate intermediates were observed during the dry heating.

This dehydration and decarbonation (Galwey and Brown 1999) behavior was further confirmed through the thermogravimetric analyses (Fig. 4). Upon heating, the ADC lost its structural water at ~100 °C and its carbonate ions at ~600 °C. The total associated weight loss for the ADC was 35 %. Of this total weight loss, 12 % weight corresponded to the release of four water molecules, while the remaining 23 % mass loss was a consequence of the carbonate decomposition and its transformation to Dy<sub>2</sub>O<sub>3</sub> at ~600 °C. From the FTIR (water and carbonate presence) and EDX (Dy:O of 2:8) data we inferred a formula for ADC corresponding to Dy<sub>2</sub>(CO<sub>3</sub>)<sub>3</sub>·xH<sub>2</sub>O. The carbonate decomposition in ADC above 550 °C followed the reaction:

$$\text{Dy}_2(\text{CO}_3)_3 \cdot x\text{H}_2\text{O} \rightarrow \text{Dy}_2\text{O}_3 + x\text{H}_2\text{O} + 3\text{CO}_2.$$

Combining all this data and taking into account the total weight loss of (35 %) and the molecular weight of Dy<sub>2</sub>O<sub>3</sub> and Dy<sub>2</sub>(CO<sub>3</sub>)<sub>3</sub>, we calculated an idealized formula of the ADC of Dy<sub>2</sub>(CO<sub>3</sub>)<sub>3</sub>·4H<sub>2</sub>O.

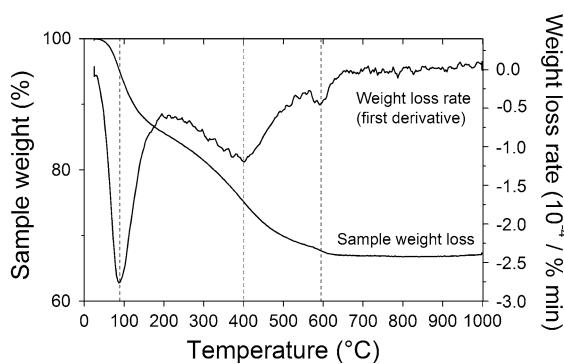


**Fig. 4** TGA (sample weight loss and weight loss rate curves) of the poorly ordered precursor. The curves show a progressive loss of water and the final carbonate decomposition at ~600 °C

The fate of ADC in solution and the formation of crystalline Dy-carbonates

When equilibrated with its original solution, regardless if at *ambient* or under *hydrothermal* conditions, the ADC was far less stable than in air and depending on reaction temperature and duration, the crystallization of four distinct Dy-carbonate phases was observed.

Within 2 days at *ambient* conditions (21 °C), ADC started to transform to a nanocrystalline (crystallite size ~7 nm; Table 1) material the XRD pattern (Fig. 5, bottom pattern) of which matched that of Dy<sub>2</sub>(CO<sub>3</sub>)<sub>3</sub>·2–3H<sub>2</sub>O, a dysprosium carbonate phase only recently described by Philippini et al. (2008). The XRD pattern of this first crystalline dysprosium carbonate is identical to other REE carbonates with a tenerite-type structure (i.e., Eu<sub>2</sub>(CO<sub>3</sub>)<sub>3</sub>·2–3H<sub>2</sub>O, Song and Rongjun 1996; Gd<sub>2</sub>(CO<sub>3</sub>)<sub>3</sub>·2–3H<sub>2</sub>O, Sungur and Kizilyalli 1983 and the fully refined Y<sub>2</sub>(CO<sub>3</sub>)<sub>3</sub>·2–3H<sub>2</sub>O, PDF 04-012-1599, Miyawaki et al. 1993). The structure of tenerites (Miyawaki et al. 1993) consists of ninefold REE-O polyhedra linked by their edges to other REE-polyhedra and also to two crystallographically independent irregular CO<sub>3</sub> groups. All these polyhedra form a structure with two channel systems, parallel to (100) and to (010), where the hydrogen atoms of the water molecules are located.

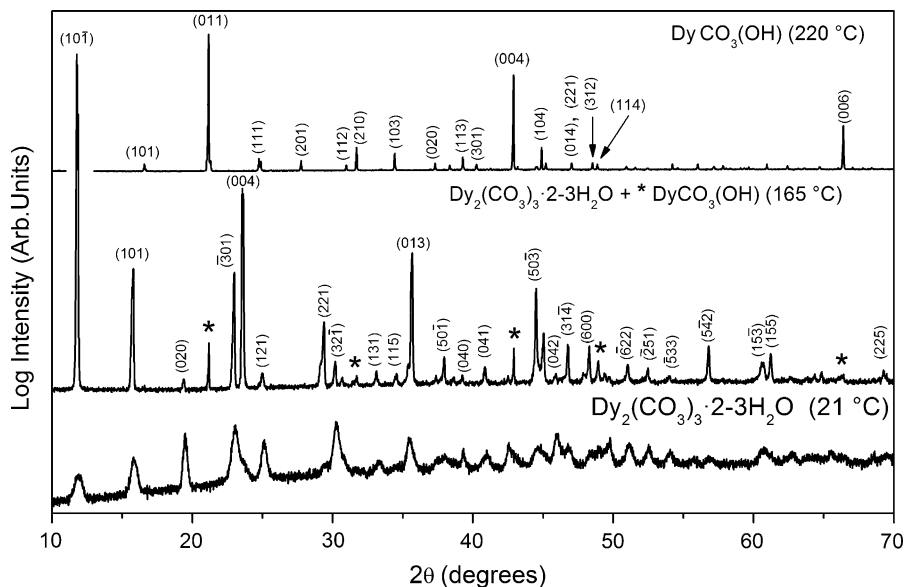
When we reacted this first crystalline Dy-carbonate, Dy<sub>2</sub>(CO<sub>3</sub>)<sub>3</sub>·2–3H<sub>2</sub>O for up to 2 months at *ambient* conditions, and re-analyzed the samples with XRD, the results revealed that this first crystalline phase remained stable at *ambient* conditions with the only observed change being an increase in crystallite size from 7 to 18 nm (Table 1). The transformation from the ADC with 4 water molecules associated with its structure (Dy<sub>2</sub>(CO<sub>3</sub>)<sub>3</sub>·4H<sub>2</sub>O) to a crystalline dysprosium carbonate trihydrate (Dy<sub>2</sub>(CO<sub>3</sub>)<sub>3</sub>·2–3H<sub>2</sub>O) shows that the first step in the crystallization of ADC occurs via a dehydration mechanism. The same dehydration was observed when the ADC was *hydrothermally* treated at 90 °C, where after 6 days, the ADC also crystallized to Dy<sub>2</sub>(CO<sub>3</sub>)<sub>3</sub>·2–3H<sub>2</sub>O with a crystallite size (16 nm; Table 1) similar to the *ambient* crystallization product after 2 months. However, *hydrothermal* treatments carried out at 165–220 °C showed substantial differences. After 2 days of reaction at 165 °C, ADC transformed to the same

**Table 1** Temperature, reaction time and identity of the solid phases, the morphologies, and the crystallite sizes calculated for all solids obtained from *ambient*, *hydrothermal*, and *dry-heated* experiments

Exp. conditions	Temp (°C)	Time (h)	Identity of the solid phase(s) (in order of abundance)	Morphology of the most abundant phase (TEM/SEM)	Crystallite size (nm)
Dry-heated	25–750	0–12 (1 °C/min ramp)	Dy <sub>2</sub> (CO <sub>3</sub> ) <sub>3</sub> ·xH <sub>2</sub> O (x < 4), amorphous (<500 °C)	Spheres	n/a
			Dy <sub>2</sub> O <sub>3</sub> (>500 °C)	(Not imaged)	202
	220	2	Dy <sub>2</sub> (CO <sub>3</sub> ) <sub>3</sub> ·xH <sub>2</sub> O (x < 4), amorphous	Spheres	n/a
	300	2	Dy <sub>2</sub> (CO <sub>3</sub> ) <sub>3</sub> ·xH <sub>2</sub> O (x < 4), amorphous	Spheres	n/a
Ambient	21	1	Dy <sub>2</sub> (CO <sub>3</sub> ) <sub>3</sub> ·4H <sub>2</sub> O, amorphous	Spheres	n/a
		48	Dy <sub>2</sub> (CO <sub>3</sub> ) <sub>3</sub> ·2–3H <sub>2</sub> O	Sheets made of needles	7
		1,440			18
Hydrothermal	90	1	Dy <sub>2</sub> (CO <sub>3</sub> ) <sub>3</sub> ·4H <sub>2</sub> O, amorphous	Spheres	n/a
		144	Dy <sub>2</sub> (CO <sub>3</sub> ) <sub>3</sub> ·2–3H <sub>2</sub> O	Sheets made of needles	16
	165	24	Dy <sub>2</sub> (CO <sub>3</sub> ) <sub>3</sub> ·xH <sub>2</sub> O (x ≤ 4), amorphous	Spheres	n/a
		48	Dy <sub>2</sub> (CO <sub>3</sub> ) <sub>3</sub> ·2–3H <sub>2</sub> O; DyCO <sub>3</sub> (OH); [Dy <sub>2</sub> O <sub>2</sub> CO <sub>3</sub> ]	Thin plates	86
	220	360	DyCO <sub>3</sub> (OH)	Rhomboheda	382
		12	DyCO <sub>3</sub> (OH); [Dy <sub>2</sub> O <sub>2</sub> CO <sub>3</sub> ]		1,137
		48	DyCO <sub>3</sub> (OH)		1,596

Chemical formulas in square brackets correspond to phases which have not been always detected in the final products. All crystallite sizes were calculated taking into account the (111) peak (28.46°) and FWHM = 0.049° from the X-ray pattern of a silicon standard (Aldrich; ICDD PDF 27-1402)

**Fig. 5** Powder X-ray diffraction patterns of the solids obtained at *ambient* (21 °C) and during *hydrothermal* (165–220 °C) treatments. The patterns could be indexed as Dy<sub>2</sub>(CO<sub>3</sub>)<sub>3</sub>·2–3H<sub>2</sub>O, Dy<sub>2</sub>(CO<sub>3</sub>)<sub>3</sub>·2–3H<sub>2</sub>O and DyCO<sub>3</sub>(OH), respectively



Dy<sub>2</sub>(CO<sub>3</sub>)<sub>3</sub>·2–3H<sub>2</sub>O, but the X-ray patterns revealed a much more crystalline material (Fig. 5, middle pattern). In these experiments, in addition to the dysprosium carbonate trihydrate observed at lower

temperatures, small peaks corresponding to a second Dy-carbonate, orthorhombic DyCO<sub>3</sub>(OH) were also observed (marked with \* in Fig 5, middle pattern; PDF 86-2229; Tahara et al. 2007; Doert et al. 1999). After

2 weeks at 165 °C,  $\text{Dy}_2(\text{CO}_3)_3 \cdot 2-3\text{H}_2\text{O}$  transformed completely to  $\text{DyCO}_3(\text{OH})$ , which had a crystallite size of just under 400 nm (Fig. 5, top pattern and Table 1). When the reaction was carried out at even higher temperatures (220 °C) the crystallization was much faster and already after 12 h the sole product was  $\text{DyCO}_3(\text{OH})$ . At this temperature in addition, a more than double crystallite size of the resulting  $\text{DyCO}_3(\text{OH})$  was observed ( $\sim 1,100$  nm). This crystallite size grew even further reaching in a size of  $\sim 1,600$  nm after 48 h of reaction (Table 1). This final, stable Dy-carbonate phase,  $\text{DyCO}_3(\text{OH})$  is a orthorhombic REE carbonate with a kozoite-type structure (Tahara et al. 2007; Doert et al. 1999) that consists of ninefold irregular Dy–O polyhedra linked to other Dy polyhedra and regular  $\text{CO}_3$  groups creating

a three dimensional network with channels along [100]. Finally, refining the pattern of the end products at 165 and 220 °C (text and Supplementary Information Fig. S2) revealed in the early stages of crystallization (i.e., 2 days at 165 °C) a minor contribution ( $\sim 1\%$ ) of a third Dy-phase that was identified as  $\text{Dy}_2\text{O}_2\text{CO}_3$  (PDF 26-0588; Kutlu and Meyer 1999; Christensen 1973).

The morphologies of all these Dy-carbonate phases were further confirmed through photomicrographs of the crystallization products (Fig. 6). Samples obtained during the *ambient* (21 °C) and low temperature (90 °C) *hydrothermal* aging, revealed that the first crystalline Dy-carbonate phase that formed from the ADC,  $\text{Dy}_2(\text{CO}_3)_3 \cdot 2-3\text{H}_2\text{O}$ , was made up of acicular crystals with a maximum length of 300 nm, which

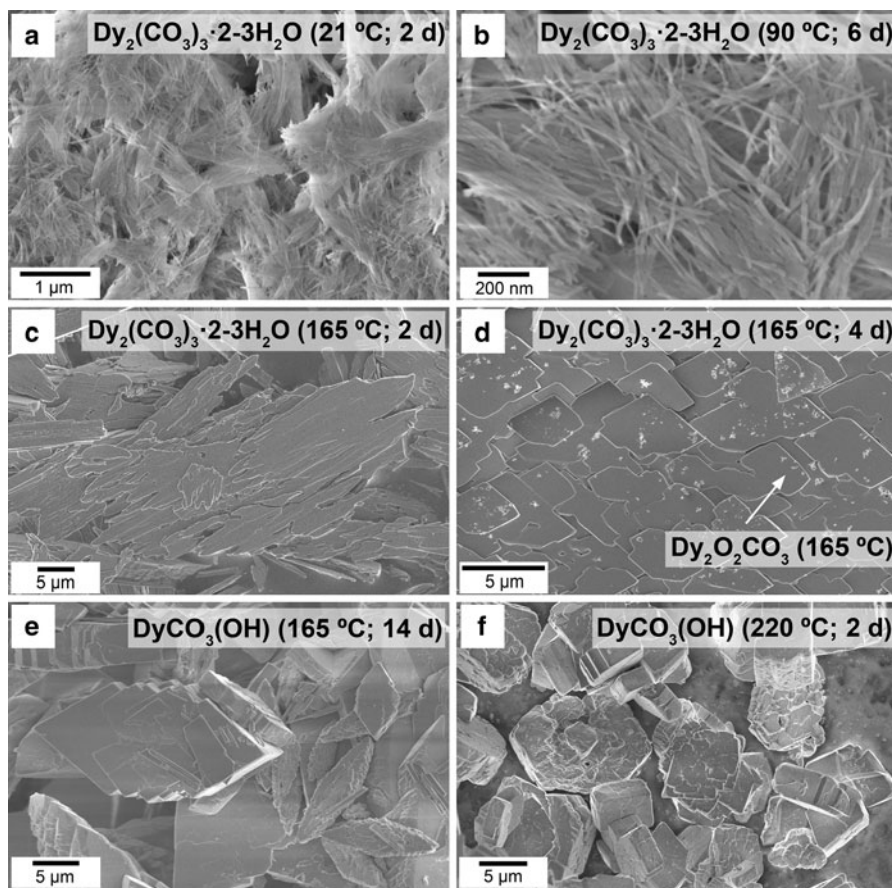


**Fig. 6** Secondary electron SEM images of the crystalline solids produced on thermal aging: **a, b** Acicular crystals/needles of  $\text{Dy}_2(\text{CO}_3)_3 \cdot 2-3\text{H}_2\text{O}$  obtained at 21 and 90 °C. **c, d** Rhombic plates of  $\text{Dy}_2(\text{CO}_3)_3 \cdot 2-3\text{H}_2\text{O}$  obtained at 165 °C, some of them

showing a second phase (*bright patches*) assumed to be  $\text{Dy}_2\text{O}_2\text{CO}_3$  (**d**). **e, f** Rhombohedral crystals of  $\text{DyCO}_3(\text{OH})$  obtained as the final product of the *hydrothermal* treatments carried out at 165 (e) and 220 °C (f)



were usually clustered in sheets (Fig. 6a–b). After 2 days of aging at 165 °C, however, the  $\text{Dy}_2(\text{CO}_3)_3 \cdot 2\text{--}3\text{H}_2\text{O}$  consisted of larger crystals (<5–20  $\mu\text{m}$  in size) with a rhombic to elongated platy morphology that in some cases still had an apparent remnant needle-like substructure (Fig. 6c) or were present as highly developed rhombic plates (Fig. 6d). On these plates, sometimes, small particles of a second phase (Fig. 6d; small bright particles) were observed, and these were assumed to be nanocrystals of the  $\text{Dy}_2\text{O}_2\text{CO}_3$  identified by XRD (Fig. 6d, Fig S1). Finally, the crystalline end product at 165–220 °C,  $\text{DyCO}_3(\text{OH})$ , was present as large and well-faceted, but aggregated rhombohedra (<35  $\mu\text{m}$  in size; Fig. 6e), or more regular well-developed rhombohedral crystals (Fig. 6f). Standardless quantification of associated EDX spectra of these final crystallization products formed at 21–90 °C ( $\text{Dy}_2(\text{CO}_3)_3 \cdot 2\text{--}3\text{H}_2\text{O}$ )

and 165–220 °C ( $\text{DyCO}_3(\text{OH})$ ) showed an approximate ratio of Dy:O which confirmed these chemical formulas.

Comparing the FTIR spectra of the crystalline phases with that of the initial ADC (Fig. 7; Table S1) shows that the carbonate vibrations are at equivalent frequencies to those found in the amorphous precursor, but that the peaks are much sharper (Fig. 7a). Furthermore, some peaks are split (e.g., for  $\text{Dy}_2(\text{CO}_3)_3 \cdot 4\text{H}_2\text{O}$  the 1,076  $\text{cm}^{-1}$  peak (marked as band 5 in Fig 7b, and Table S1) splits into two peaks at 1,091 and 1,064  $\text{cm}^{-1}$  in  $\text{Dy}_2(\text{CO}_3)_3 \cdot 2\text{--}3\text{H}_2\text{O}$  (bands 10 and 11 in Fig. 7b; Table S1) or transformed into a single much sharper vibration at 1,093  $\text{cm}^{-1}$  in  $\text{DyCO}_3(\text{OH})$ . This splitting in  $\text{Dy}_2(\text{CO}_3)_3 \cdot 2\text{--}3\text{H}_2\text{O}$  and the absence of some of these bands in  $\text{DyCO}_3(\text{OH})$  can be accounted for by the structural differences between tengerites and kozoites. Tengerite-type carbonates ( $\text{REE}_2(\text{CO}_3)_3 \cdot 2\text{--}3\text{H}_2\text{O}$ ) have two crystallographically independent  $\text{CO}_3$  groups which are irregular (different distances of C–O bonds in the same  $\text{CO}_3$  group), while kozoite-type carbonates ( $\text{REECO}_3(\text{OH})$ ) only have one crystallographically independent regular  $\text{CO}_3$  group. Furthermore, the broad (O–H stretching) band observed between 2,500 and 3,700  $\text{cm}^{-1}$  that corresponds to structural water was still present in  $\text{Dy}_2(\text{CO}_3)_3 \cdot 2\text{--}3\text{H}_2\text{O}$  (band marked with 1 in lower two spectra in Fig. 7a), but this broad band has been replaced in  $\text{DyOHCO}_3$  with two narrow peaks at 3,503 and 3,479  $\text{cm}^{-1}$  (bands 16, 17 in upper spectra Fig 7a, Table S1) indicative of O–H stretches in highly crystalline materials (Farmer 1974).

Magnetic measurements of ADC,  $\text{Dy}_2(\text{CO}_3)_3 \cdot 4\text{H}_2\text{O}$ , and the *hydrothermally* treated stable crystalline end product,  $\text{DyCO}_3(\text{OH})$ , both show simple paramagnetic behaviors over the temperature range studied (Fig. 8). The temperature dependence of the molar magnetic susceptibility,  $\chi$ , follows the Curie–Weiss law (Van Vleck 1952) with a Weiss temperature,  $\theta_p$  of –4.33 K for ADC and –5.32 K for  $\text{DyCO}_3(\text{OH})$ . Both phases have similar effective magnetic moments ( $\mu_{\text{eff}} = 8.17$  and 10.65  $\mu_B/\text{Dy}$  ion, respectively) with the higher value being similar to the effective magnetic moment expected for the free  $\text{Dy}^{3+}$  ion ( $\mu_{\text{eff}} = 10.65 \mu_B$ ) (Van Vleck 1952). The lower  $\mu_{\text{eff}}$  for ADC may be a result of an enhanced crystal field around the ion, according to the van Vleck formalism for describing paramagnetic rare earth compounds (Van Vleck 1952). The reduced effective

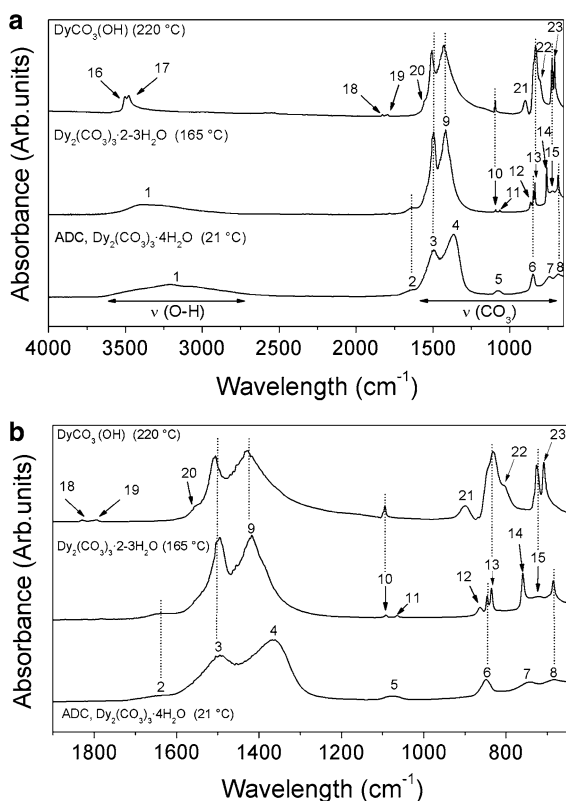


**Fig. 7** **a** FTIR spectra of the amorphous precursor (*bottom*) and the products of the *hydrothermal* experiment obtained at 165 °C (*middle*) and 220 °C (*top*). Main molecular/lattice absorption bands are indicated by numbers above the spectra. **b** Detail of the FTIR bands located between 650 and 1,850  $\text{cm}^{-1}$ . Details of the band assignments are discussed in Table S1 and the text

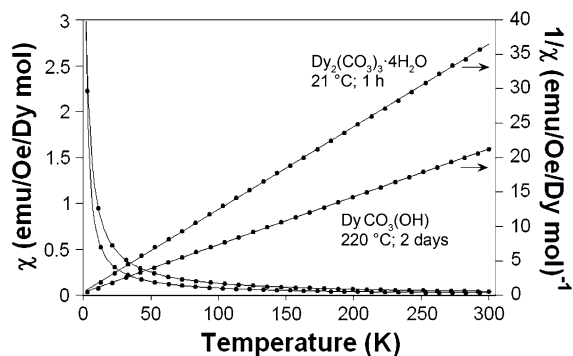


**Fig. 8** Temperature dependence of molar magnetic susceptibility ( $\chi$ ) and its inverse  $1/\chi$  showing a paramagnetic behavior in both the amorphous precursor phase ( $\text{Dy}_2(\text{CO}_3)_3 \cdot 4\text{H}_2\text{O}$ ) and final crystalline product ( $\text{DyCO}_3(\text{OH})$ ) in the hydrothermal treatment

moments of the paramagnetic ion seem to suggest that the overall crystalline electric field splitting of the  $\text{Dy}^{3+}$  ion in the amorphous material is larger than that of the crystalline material (Blanco et al. 1992).

Is amorphous dysprosium carbonate special?

Our experiments evidence the formation of a variety of Dy carbonates with different stability ranges, compositions, and structures. Table 1 shows a summary of the results, including reaction times, identities, morphologies, and crystallinity of the products.

Some of the characteristics of the ADC are comparable to other amorphous precursors like amorphous calcium carbonate (ACC; Radha et al. 2010; Rodriguez-Blanco et al. 2008) or amorphous calcium, aluminum, and iron phosphates (Roncal-Herrero et al. 2009; Eanes 2001). All these poorly ordered nanoparticles show spherical morphologies and similar sizes. ACC and ADC have also almost equivalent XRD patterns with intensities at  $\sim 20$ – $30$  and  $45^\circ 2\theta$ . An important difference is the degree of ADC hydration identified here. We showed that ADC has four water molecules per formula unit and this is substantially more water in the structure compared to other amorphous carbonate phases. For example, ACC is known to contain  $\sim 1$  water molecule per formula unit (Radha et al. 2010; Huang et al. 2007), while when the ACC is magnesium rich this value can reach 1.37 water molecules (Rodriguez-Blanco et al. 2009).

However, the most striking character of the ADC we produced in this study is its long-term stability in

air and even in solution compared to amorphous calcium carbonate, ACC. ACC remains stable in air for maximum 3 days, but only if prepared by a fast quench/dry-solvent filtration approach (Rodriguez-Blanco et al. 2008), while ADC remained stable for long time periods and even at higher temperatures. The resistance of ADC to dehydrate and crystallize when heated dry is remarkable for such a hydrated, amorphous, and carbonate precursor.

Interestingly, ADC is also more stable than other amorphous precursors when reacted in solution at ambient conditions. Our results demonstrate that ADC aged in solution crystallized only after  $\sim 2$  days and then it transformed to a poorly crystalline phase,  $\text{Dy}_2(\text{CO}_3)_3 \cdot 2$ – $3\text{H}_2\text{O}$ . This is in contrast to the calcium and calcium–magnesium carbonate systems, where the transformation of the amorphous precursors at equivalent conditions in solution has been shown to be much faster: the transformation of ACC to crystalline  $\text{CaCO}_3$  in solution occurs in 1–2 min at ambient temperature (Ogino et al. 1987) and is considered to involve a dehydration process (Rodriguez-Blanco et al. 2011a, b). The crystallization of Mg-doped ACC although it occurs at a slower pace compared to ACC (Rodriguez-Blanco et al. 2011a, b; Politi et al. 2010) it is still much faster than ADC. Furthermore, in the presence of Mg the energy needed to dehydrate the Mg ion is higher compared to the Ca ion (Di Tommaso and de Leeuw 2010). The exceptionally high stability of ADC in the dry state suggests that a high activation energy is required to dehydrate the Dy ion before crystallization can occur. This is consistent with the observations that many dysprosium-bearing compounds are highly hygroscopic (Annis et al. 1985; Herdman and Salmon 1991; Sankaranarayanan and Gajbhiye 1989).

Our study, however, clearly shows that the crystallization of Dy-bearing carbonates necessitates the initial formation of a highly hydrated, amorphous precursor, and that although Dy-bearing tengerites can form at ambient temperatures, their crystallization is favoured during hydrothermal processes. However, tengerite-type Dy-carbonates are unstable and transform to kozoite-type carbonates via a series of dehydration processes. Our hydrothermal experiments shows that orthorhombic  $\text{DyCO}_3(\text{OH})$  is the final stable phase at the temperature range studied (21–220 °C) and it is known that it would transform to  $\text{Dy}_2\text{O}_2\text{CO}_3$  at higher ( $>450$  °C) temperatures

(Kutlu and Meyer 1999; Christensen 1973). Although this study is focused in Dy-bearing compounds, our results can be extrapolated to other REE-bearing tengerites (Miyawaki et al. 1993) and kozoites (Miyawaki et al. 2000), which have been suggested to form in nature also as a consequence of hydrothermal process.

## Conclusions

We show that the precipitation of dysprosium carbonates from solution at room temperature proceeds via the formation of a highly hydrated, nanoparticulate, and ADC phase, ADC with a formula of  $\text{Dy}_2(\text{CO}_3)_3 \cdot 4\text{H}_2\text{O}$ . This ADC is exceptionally stable in air, even at near carbonate decomposition temperatures. In a dry state, ADC progressively loses its water upon heating to 550 °C and interestingly, it does not transform to a crystalline Dy-carbonate, but crystallized to a Dy-oxide,  $\text{Dy}_2\text{O}_3$ , through dehydration and carbonate calcination. When reacted in solution the ADC also remains stable before transforming into crystalline Dy-tengerite,  $\text{Dy}_2(\text{CO}_3)_3 \cdot 2-3\text{H}_2\text{O}$ . The stability and crystallinity of this first crystalline Dy-carbonate is strongly temperature-dependent: under hydrothermal conditions it transforms to Dy-kozoite,  $\text{DyCO}_3\text{OH}$ , in hours or days, but at ambient temperature it remains stable as a poorly crystalline  $\text{Dy}_2(\text{CO}_3)_3 \cdot 2-3\text{H}_2\text{O}$  for months. Neither the amorphous nor the crystalline phases present any long-range magnetic order from 300 K down to 1.8 K. This study also suggests that other stable REE-bearing amorphous precursors may directly form from solution. Such amorphous materials would have many potential applications in modern technologies. This is particularly important because REE are key materials in the production of high-technology devices and also are essential to develop clean energy products.

**Acknowledgments** This research was supported by the Marie Curie EU-FP6 MINGRO Research and Training Network under contract MRTNCT-2006-035488. The authors would like to thank the Cohen Laboratories in the School of Earth and Environment, the Leeds Electron Microscopy and Spectroscopy Centre (LEMAS) at the Faculty of Engineering (University of Leeds), and the Spanish Ministry of Science and Innovation (MICINN-12-MAT2011-27573-C04-02). The help of Imanol De Pedro del Valle with the magnetic measurements from the University of Cantabria (Spain) is acknowledged.

## References

- Adachi GY, Imanaka N, Tamura S (2010) Research trends in rare earths: a preliminary analysis. *J Rare Earth* 28: 843–846. doi:10.1016/S1002-0721(09)60207-6
- Annis BK, Hahn RL, Narten AH (1985) Hydration of the  $\text{Dy}^{3+}$  ion in dysprosium chloride solutions determined by neutron diffraction. *J Chem Phys* 82:2086–2091. doi:10.1063/1.448345
- Bauer D, Diamond D, Li J, McKittrick M, Sandalow D, Telleen P (2011) Critical Materials Strategy. US Department of Energy. Washington DC, 2011. <http://energy.gov/pi/office-policy-and-international-affairs/downloads/2011-critical-materials-strategy>
- Blanco JA, Gignoux D, Schmitt D (1992) Crystal field and magnetic properties of the tetragonal  $\text{TbNi}_2\text{Si}_2$  compound. *Z Phys B Condens. Matter* 89:343–350. doi:10.1007/BF01318166
- Bolze J, Peng B, Dingenouts N, Panine P, Narayanan T, Ballauff M (2002) Formation and growth of amorphous colloidal  $\text{CaCO}_3$  precursor particles as detected by time-resolved SAXS. *Langmuir* 18:8364–8369. doi:10.1021/la025918d
- Bots P, Rodriguez-Blanco JD, Roncal-Herrero T, Shaw S, Benning LG (2012) Mechanistic insights into the crystallization of amorphous calcium carbonate to vaterite. *Cryt Growth Des* 12:3806–3814. <http://dx.doi.org/10.1021/cg300676b>
- Brečević L, Nielsen AE (1989) Solubility of amorphous calcium carbonate. *J Cryst Growth* 98:504–510. doi:10.1016/0022-0248(89)90168-1
- Bünzli JCG, Piguet C (2005) Taking advantage of luminescent lanthanide ions. *Chem Soc Rev* 34:1048–1077. doi:10.1039/b406082m
- Buschow KHJ (1984) Amorphous alloys. In: Gschneidner KA, Eyring L (eds) Handbook on the physics and chemistry of rare earths, vol 7. Elsevier, Amsterdam, pp 265–443. doi:10.1016/S0168-1273(84)07005-7
- Caro PE, Sawyer JO, Eyring L (1972) The infrared spectra of rare earth carbonates. *Spectrochim Acta* 8:1167–1173. doi:10.1016/0584-8539(72)80088-6
- Charles RG (1965) Rare-earth carbonates prepared by homogeneous precipitation. *J Inorg Nucl Chem* 27:1489–1493. doi:10.1016/0022-1902(65)80008-2
- Christensen AN (1973) Hydrothermal preparation and magnetic properties of  $\text{Dy}_2\text{O}_2\text{CO}_3$ ,  $\text{Ho}_2\text{O}_2\text{CO}_3$ ,  $\text{Er}_2\text{O}_2\text{CO}_3$  and  $\text{Yb}_2\text{O}_2\text{CO}_3$ . *Acta Chem Scand* 27:1835–1837. doi:10.3891/acta.chem.scand.27-1835
- Coelho AA (2003) TOPAS: general profile and structure analysis software for powder diffraction data
- Combes C, Rey C (2010) Amorphous calcium phosphates: synthesis, properties and uses in biomaterials. *Acta Biomater* 6:3362–3378. doi:10.1016/j.actbio.2010.02.017
- Di Tommaso D, de Leeuw NH (2010) Structure and dynamics of the hydrated magnesium ion and of the solvated magnesium carbonates: insights from first principles simulations. *Phys Chem Chem Phys* 12:894–901. doi:10.1039/b915329b
- Doert T, Rademacher O, Getzschmann J (1999) Crystal structure of dysprosium hydroxide carbonate  $\text{DyOHCO}_3$ . *Z Krist New Cryst St* 214:11–12

- Eanes ED (2001) Amorphous calcium phosphate. *Monogr Oral Sci* 18:130–147. doi:[10.1159/000061652](https://doi.org/10.1159/000061652)
- Farmer VC (1974) *The Infrared Spectra of Minerals*. Mineralogical Society of Great Britain & Ireland. Mineralogical Society Monograph 4
- Firsching FH, Mohammadzadei J (1986) Solubility products of the rare-earth carbonates. *J Chem Eng Data* 31:40–42. doi:[10.1021/je00043a013](https://doi.org/10.1021/je00043a013)
- Galwey AK, Brown ME (1999) Decomposition of carbonates. Thermal decomposition of ionic solids. Elsevier B.V. Ed, In, pp 345–364
- Gasgnier M (1991) Rare-earth elements in permanent magnets and superconducting compounds and alloys (except new high  $T_c$  ceramics) as thin films, thin crystals and thinned bulk materials. *J Mater Sci* 26:1989–1999. doi:[10.1007/BF00549157](https://doi.org/10.1007/BF00549157)
- Goodwin A, Michel FM, Phillips BL, Keen DA, Dove MT, Reeder RJ (2010) Nanoporous structure and medium-range order in synthetic amorphous calcium carbonate. *Chem Mater* 22:3197–3205. doi:[10.1021/cm100294d](https://doi.org/10.1021/cm100294d)
- Herdman GJ, Salmon PS (1991) Dynamics of water protons in concentrated  $Ga^{3+}$ ,  $Al^{3+}$ ,  $Fe^{3+}$  and  $Dy^{3+}$  aqueous solutions: a study using incoherent quasi-electric neutron scattering. *J Am Chem Soc* 113:2930–2939. doi:[10.1021/ja00008a022](https://doi.org/10.1021/ja00008a022)
- Huang CH (2010) Rare earth coordination chemistry: Fundamentals and applications. John Wiley & Sons, Singapore 2010
- Huang SC, Naka K, Chujo Y (2007) A carbonate controlled-addition method for amorphous calcium carbonate spheres stabilized by poly(acrylic acid)s. *Langmuir* 23:12086–12095. doi:[10.1021/la701972n](https://doi.org/10.1021/la701972n)
- Jones AP, Wall F (1996) Williams CT (1996) Rare earth minerals: chemistry, origin and ore deposits. Chapman & Hall, London
- Kanamori J (2006) Rare earth elements and magnetism in metallic systems. *J Alloy Compd* 408–412:2–8. doi:[10.1016/j.jallcom.2005.04.103](https://doi.org/10.1016/j.jallcom.2005.04.103)
- Kutlu I, Meyer G (1999) Basische Carbonate des Dysprosiums:  $Dy_2O_2(CO_3)$  und  $Dy(OH)(CO_3)$ . *Z Anorg Allg Chem* 625:402–406. doi:[10.1002/\(SICI\)1521-3749\(199903\)625:3<402:AID-ZAAC402>3.0.CO;2-S](https://doi.org/10.1002/(SICI)1521-3749(199903)625:3<402:AID-ZAAC402>3.0.CO;2-S)
- Leskelä M, Niinistö L (1986) Inorganic complex compounds I. In: Gschneidner KA, Eyring L (eds) *Handbook of the physics and chemistry of rare earths*, vol 8. Elsevier, Amsterdam, pp 203–334
- McHenry ME, Laughlin DE (2000) Nano-scale materials development for future magnetic applications. *Acta Mater* 48:223–238. doi:[10.1016/S1359-6454\(99\)00296-7](https://doi.org/10.1016/S1359-6454(99)00296-7)
- McHenry ME, Willard MA, Laughlin DE (1999) Amorphous and nanocrystalline materials for applications as soft magnets. *Prog Mater Sci* 44:291–433. doi:[10.1016/S0079-6425\(99\)00002-X](https://doi.org/10.1016/S0079-6425(99)00002-X)
- Meldrum FC, Cölfen H (2008) Controlling mineral morphologies and structures in biological and synthetic systems. *Chem Rev* 108:4332–4432. doi:[10.1021/cr8002856](https://doi.org/10.1021/cr8002856)
- Meldrum FC, Sear RP (2008) Now you see them. *Science* 322:1802–1803. doi:[10.1126/science.1167221](https://doi.org/10.1126/science.1167221)
- Michiba K, Tahara T, Nakai I, Miyawaki R, Matsubara S (2011) Crystal structure of hexagonal  $RE(CO_3)OH$ . *Z Kristallogr* 226:518–530. doi:[10.1524/zkri.2011.1222](https://doi.org/10.1524/zkri.2011.1222)
- Miyawaki R, Kuriyama J, Nakai I (1993) The redefinition of tengerite-(Y),  $Y_2(CO_3)_3 \cdot 2-3H_2O$ , and its crystal structure. *Am Mineral* 78:425–432
- Miyawaki R, Matsubara S, Yokoyama K, Takeuchi K, Terada Y, Nakai I (2000) Kozoite-(Nd),  $Nd(CO_3)(OH)$ , a new mineral in an alkali olivine basalt from Hizen-cho, Saga Prefecture, Japan. *Am Mineral* 85:1076–1081
- Ogino T, Suzuki T, Sawada K (1987) The formation and transformation mechanism of calcium carbonate in water. *Geochim Cosmochim Acta* 51:2757–2767. doi:[10.1016/0016-7037\(87\)90155-4](https://doi.org/10.1016/0016-7037(87)90155-4)
- Patterson AL (1939) The Scherrer formula for X-ray particle size determination. *Phys Rev* 56:978–982. doi:[10.1103/PhysRev.56.978](https://doi.org/10.1103/PhysRev.56.978)
- Philippini V, Vercoeur T, Chaussé A, Vitorge P (2008) Precipitation of  $AlN(CO_3)_2 \cdot xH_2O$  and  $Dy_2(CO_3)_3 \cdot xH_2O$  compounds from aqueous solutions for  $A^{3+} = Li^+, Na^+, K^+, Cs^+, NH_4^+$  and  $Ln^{3+} = La^{3+}, Nd^{3+}, Eu^{3+}, Dy^{3+}$ . *J Solid State Chem* 181:2143–2154. doi:[10.1002/chin.200852018](https://doi.org/10.1002/chin.200852018)
- Politi Y, Batchelor DR, Zaslansky P, Chmelka BF, Weaver JC, Sagi I, Weiner S, Addadi L (2010) Role of magnesium ion in the stabilization of biogenic amorphous calcium carbonate: a structure-function investigation. *Chem Mat* 22:161–166. doi:[10.1021/cm902674h](https://doi.org/10.1021/cm902674h)
- Radha AV, Forbes TZ, Killian CE, Gilbert PUPA, Navrotsky A (2010) Transformation and crystallization energetics of synthetic and biogenic amorphous calcium carbonate. *P Natl Acad Sci USA* 107:16348–16443. doi:[10.1073/pnas.1009959107](https://doi.org/10.1073/pnas.1009959107)
- Refat MS (2004) A novel method for the synthesis of rare earth carbonates. *Syn React Inorg Met* 34:1605–1613. doi:[10.1081/SIM-200026601](https://doi.org/10.1081/SIM-200026601)
- Rodriguez-Blanco JD, Shaw S, Benning LG (2008) How to make ‘stable’ ACC: protocol and preliminary structural characterization. *Mineral Mag* 72:283–286. doi:[10.1180/minmag.2008.072.1.283](https://doi.org/10.1180/minmag.2008.072.1.283)
- Rodriguez-Blanco JD, Shaw S, Benning LG (2009) The realtime kinetics and mechanisms of nucleation and growth of dolomite from solution. *Geochim et Cosmochim Acta*, 73, A1111. doi:[10.1016/j.gca.2009.05.014](https://doi.org/10.1016/j.gca.2009.05.014)
- Rodriguez-Blanco JD, Bots P, Roncal-Herrero T, Shaw S, Benning LG (2011) The role of pH and Mg in the stability and crystallization of amorphous calcium carbonate. *J Alloy Compd* 536: S477–S479. <http://dx.doi.org/10.1016/j.jallcom.2011.11.057>
- Rodriguez-Blanco JD, Shaw S, Benning LG (2011b) The kinetics and mechanisms of amorphous calcium carbonate (ACC) crystallization to calcite, via vaterite. *Nanoscale* 3:265–271. doi:[10.1039/C0NR00589D](https://doi.org/10.1039/C0NR00589D)
- Roncal-Herrero T, Rodriguez-Blanco JD, Benning LG, Oelkers EH (2009) Precipitation of iron and aluminum phosphates directly from aqueous solution as a function of temperature from 50 to 200 °C. *Cryst Growth Des* 9:5197–5205. doi:[10.1021/cg900654m](https://doi.org/10.1021/cg900654m)
- Roncal-Herrero T, Rodriguez-Blanco JD, Oelkers EH, Benning LG (2011) The direct precipitation of rhabdophane ( $REPO_4 \cdot nH_2O$ ) nano-rods from acidic aqueous solutions at 5–100°C. *J Nanopart Res* 13:4049–4062. doi:[10.1007/s11051-011-0347-6](https://doi.org/10.1007/s11051-011-0347-6)



- Salavati-Niasari M, Javidi J, Davar F, Fazl AA (2010) Sonochemical synthesis of  $Dy_2(CO_3)_3$  nanoparticles and their conversion to  $Dy_2O_3$  and  $Dy(OH)_3$ : effects of synthesis parameters. *J Alloy Compd* 503:500–506. doi:[10.1016/j.jallcom.2010.05.041](https://doi.org/10.1016/j.jallcom.2010.05.041)
- Sankaranarayanan VK, Gajbhiye NS (1989) Thermal decomposition of dysprosium iron citrate. *Thermochim Acta* 153:337–348. doi:[10.1016/0040-6031\(89\)85448-6](https://doi.org/10.1016/0040-6031(89)85448-6)
- Song L, Rongjun M (1996) Synthesis and structure of hydrated europium carbonate. *J Cryst Growth* 169:190–192. doi:[10.1016/0022-0248\(96\)00290-4](https://doi.org/10.1016/0022-0248(96)00290-4)
- Song L, Rongjun MA (2006) Synthesis of hydrated praseodymium, samarium, gadolinium and dysprosium carbonates. *J Rare Earth* 24:358–361
- Sungur A, Kizilyalli M (1983) Synthesis and structure of  $Gd_2(CO_3)_3 \cdot nH_2O$  ( $n = 2,3$ ). *J Less Common Met* 93:419–423. doi:[10.1016/0022-5088\(83\)90197-2](https://doi.org/10.1016/0022-5088(83)90197-2)
- Tahara T, Nakai I, Miyawaki R, Matsubara S (2007) Crystal chemistry of  $RE(CO_3)OH$ . *Z Kristallogr* 222:326–334. doi:[10.1524/zkri.2007.222.7.326](https://doi.org/10.1524/zkri.2007.222.7.326)
- Tobler DJ, Benning LG (2011) The microbial diversity in Icelandic hot springs: temperature, salinity, pH and sinter growth rate effects. *Extremophiles* 15:473–485. doi:[10.1007/s00792-011-0378-z](https://doi.org/10.1007/s00792-011-0378-z)
- Tobler DJ, Shaw S, Benning LG (2009) Quantification of initial steps of nucleation and growth of silica nanoparticles: an in situ SAXS and DLS study. *Geochim Cosmochim Acta* 73:5377–5393. doi:[10.1016/j.gca.2009.06.002](https://doi.org/10.1016/j.gca.2009.06.002)
- Van Driessche AES, Benning LG, Rodriguez-Blanco JD, Osorio M, Bots P, García-Ruiz JM (2012) The role and implications of bassanite as a stable precursor phase to gypsum precipitation. *Science* 336:69–72. doi:[10.1126/science.1215648](https://doi.org/10.1126/science.1215648)
- Van Vleck JH (1952) The theory of electric and magnetic susceptibilities. Oxford University Press, London
- Xu AW, Fang YP, You LP, Liu HQ (2003) A simple method to synthesize  $Dy(OH)_3$  and  $Dy_2O_3$  nanotubes. *J Am Chem Soc* 125:1494–1495. doi:[10.1021/ja029181q](https://doi.org/10.1021/ja029181q)
- Yan CH, Yan ZG, Du YP, Shen J, Zhang C, Feng W (2011) Controlled synthesis and properties of rare earth nanomaterials. In: Gschneidner KA, Bunzli JCG, Pecharsky VK (eds) Handbook on the physics and chemistry of rare earths, vol 41. Elsevier, Amsterdam, pp 275–472
- Yang KF, Fan HR, Santosh M, Hu FF, Wang KY (2011) Mesoproterozoic carbonatitic magmatism in the Bayan Obo deposit, Inner Mongolia, north China: constraints for the mechanism of super accumulation of rare earth elements. *Ore Geol Rev* 40:122–131. doi:[10.1016/j.oregeorev.2011.05.008](https://doi.org/10.1016/j.oregeorev.2011.05.008)
- Zhang J, Lim KY, Feng YP, Li Y (2007) Fe–Nd–B–based hard magnets from bulk amorphous precursor. *Scripta Mater* 56:943–946. doi:[10.1016/j.scriptamat.2007.02.016](https://doi.org/10.1016/j.scriptamat.2007.02.016)
- Zyman ZZ, Rokhmistrov DV, Glushko VI (2010) Structural and compositional features of amorphous calcium phosphate at the early stage of precipitation. *J Mater Sci Mater Med* 21:123–130. doi:[10.1007/s10856-009-3856-4](https://doi.org/10.1007/s10856-009-3856-4)